CrossMark

A novel segmentation model for medical images with intensity inhomogeneity based on adaptive perturbation

Haiping Yu[1] · Fazhi He[2] · Yiteng Pan[1]

Abstract

In medical field, it remains challenging to accurately segment medical images due to low contrast, complex noises and intensity inhomogeneity. To overcome these obstacles, this paper provides a novel edge-based active contour model (ACM) for medical image segmentation. Specifically, an accurate regularization approach is presented to maintain the level set function with a signed distance property, which guarantees the stability of the evolution curve and the accuracy of the numerical computation. More significantly, an adaptive perturbation is integrated into the framework of the edge-based ACM. The perturbation technique can balance the stability of curve evolution and the accuracy of segmentation, which is key for segmenting medical images with intensity inhomogeneity. A number of experiments on both artificial and real medical images demonstrate that the proposed segmentation model outperforms state-of-the-art methods in terms of robustness to noise and segmentation accuracy.

1 Introduction

Medical image segmentation is a hot research area in computer vision and image processing [5, 7, 21, 32, 34, 51, 56, 76, 83, 85]. Accurate segmentation results are applied in the field

✉ Fazhi He
fzhe@whu.edu.cn

Haiping Yu
seaping@whu.edu.cn

Yiteng Pan
panyiteng@whu.edu.cn

[1] School of Computer Science, Wuhan University, Wuhan, China

[2] State Key Lab of Software Engineering, School of Computer Science, Wuhan University, Wuhan, China

of image understanding, such as for surgical planning, abnormality detection and disease prediction [11, 64, 88]. Manual image segmentation not only relies on experienced experts but also is time-consuming. Therefore, researchers have proposed many automatic segmentation methods, including clustering based methods [17, 19, 20], learning-based methods [26, 63], superpixel-based methods [1, 24] and active contour models(ACMs) [2, 45, 52, 73, 74, 84]. In recent years, ACMs have been increasingly and widely used in image processing. The basic idea of ACMs can extract a desired object by using en evolution curve. They can be divided into two types of models: explicit ACMs [15, 25, 62] and implicit ACMs [8, 28, 48, 49, 61, 78]. Recently, level set methods(LSMs), as typical implicit active contour models, have been widely used for image segmentation. LSMs provide convenient shape representation for numerical computations and can easily handle topological changes in curve evolution in a very conventional way. In addition, LSMs do not parameterize the evolution curve.

However, traditional LSMs have the following limitations.

(1) High computational complexity: Level set implementation is based on a higher dimension, which increases the computational cost. If the image size is N, the computational complexity is $O(N * N)$.

(2) Irregular evolution function: During the level set evolution, numerical errors appear occasionally, which causes the irregular evolution function. The main reason is the the irregularity of the level set function(LSF). Thus, it is very significant for LSF to maintain the signed distance property. This property ensure the correctness of the numerical calculation and the stability of evolution.

(3) Low robustness to noise: The traditional LSMs are inherently sensitive to noise for segmenting noisy images. Recently, some improved level set methods with a certain effect on segmenting noisy images have been developed [57]. For example, reference [30] adopted an edge indicator function g to reduce noise (see Eq. 1). Niu et al. used a local similarity factor to resist the influence of noise [45]:

$$g = \frac{1}{1 + |\nabla G_\sigma * I|^2} \tag{1}$$

here, I is an image, G_σ is a Gaussian kernel with deviation σ, and g is the edge indicator function.

(4) Challenge of intensity inhomogeneous image segmentation: To segmente an image with intensity inhomogeneity, several methods based on LSMs have been presented in the literature [3, 23, 31, 43, 55, 59, 81]. In the reference [43], the model approximated the image intensity with a piecewise smooth function, which achieved the desired segmentation results for images with intensity inhomogeneity. However, it was very difficult to solve the energy functional due to its non-convexity [39, 46]. In addition, the model was very time-consuming and limited in practical applications.

(5) Deficiency of locality: Existing LSMs lack locality properties. However, some improved LSMs have the feature of a signed distance profile near the zero level set, which does not guarantee the uniqueness of local properties. A localizing region-based model has been proposed in the literature [6, 18, 27, 54].

To address the aforementioned problems, this paper presents a hybrid level set model for image segmentation. The main contribution of this paper includes three aspects:

(1) We first utilize an efficient diffusion function to regularize the level set evolution, which ensure the correctness of the numerical calculation and the stability of the curve evolution.

(2) Second, in order to balance the stability of the curve evolution and the accuracy of the segmentation, a perturbation factor is constructed to integrate the external energy functional of the curve evolution.

(3) Third, a new edge indicator function is proposed to resist the noise of the image while preserving image edge detail to a large extent.

(4) Finally, a large number of experimental results for synthetic and medical images show the superiority of our model in terms of anti-noise ability and segmentation accuracy. In addition, comparisons with well-known segmentation models show that our model is more efficient and robust to noise.

The remainder of this paper is organized as follows: Section 2 reviews previous research. A new segmentation model based on adaptive perturbation is proposed in Section 3. The experimental results are given in Section 4. Section 5 discusses the evaluation of the proposed model. Finally, conclusion and future works are discussed in Section 6.

2 Related works

In image processing fields, LSMs have been widely used to solve image segmentation problems, however, their applications have been troubled with the irregularities of the LSF in segmenting images with intensity inhomogeneity. Therefore, many improved LSMs have been proposed, such as the reference [29–31, 57, 78, 79, 81]. To sum up, the improved LSMs is divided into two classes: re-initialization-based LSMs and variational LSMs without re-initialization. In this section, we will introduce two categories of models for image segmentation: re-initialization-based LSMs and variational LSMs without re-initialization. Then, we describe the two categories and their limitations for segmenting images with intensity inhomogeneity.

2.1 Re-initialization based level set method

In the traditional level set method, high-dimensional implicit functions tend to be sharp or flat during the evolution, which results in numerical inaccuracy. To avoid these defects, one remedy is to initialize the implicit function as a signed distance function(SDF) periodically during the curve evolution. The work in [47] first proposed to initialize the LSF as $\phi(x) = 1 \pm dist^2(x)$. Here, $dist^2(x)$ represents a distance function. The standard re-initialization equation is defined as follows:

$$\frac{\partial \phi}{\partial t} = sign(\phi_0)(1 - |\nabla \phi|) \tag{2}$$

where ϕ_0 is a re-initialization function, ϕ is the high dimensional implicit function, the function of $sign(\cdot)$ represents the sign function [50, 80], and t is a time step.

The re-initialization method plays a significant role in maintaing the stability of curve evolution. In practical applications, there are three shortcomings:

(1) Problem of re-initialization execution: In the evolution processing, how and when to initialize the LSF to a sign distance function remain unsolved problems.

(2) Time step constraints: When the time step is larger, the LSF's ϕ may wander irregularly in some iteration steps and become far, form an SDF resulting in inaccurate segmentation results. By contrast, the shorter the time step, the higher the accuracy, and the higher the time consumption.

(3) High time consumption: Ideally, the re-initialization function will allow the LSF to have the property of a signed function to ensure stable curve evolution. Because of its ad-hoc manner, the time consumption is excessively high. In addition, the LSF is compelled to be an SDF, which cannot guarantee stability.

2.2 Variational LSMs without re-initialization

To solve the defects of the re-initialization based LSM, researchers have proposed some variational LSMs without re-initialization to adjust the level set function during curve evolution. Li et al. proposed a variational formulation as a penalty term to eliminate the process of re-initialization [28, 30]. The penalty term $P(\phi)$ is defined as follows:

$$P(\phi) = \frac{1}{2} \int_{\Omega} (|\nabla \phi| - 1)^2 dx \tag{3}$$

The gradient flow of $P(\phi)$ is obtained as follows:

$$\frac{\partial \phi}{\partial t} = -\frac{\partial P}{\partial t} = div(D \nabla \phi) \tag{4}$$

here, D is a diffusion rate. The penalty term can successfully regularize the variational LSF.

For variational LSMs, Li et al. proposed two diffusion rates to regularize the level set evolution. These rates $D_i (i = 1, 2)$ are defined as follows:

$$D1 = 1 - \frac{1}{|\nabla \phi|}, \quad |\nabla \phi| > 0 \tag{5}$$

$$D2 = \begin{cases} \frac{sin(2\pi|\nabla\phi|)}{2\pi|\nabla\phi|}, & 0 < |\nabla\phi| \le 1 \\ 1 - \frac{1}{|\nabla\phi|}, & |\nabla\phi| > 1 \end{cases} \tag{6}$$

where, D_1 and D_2 are called $DRLSE_1$ and $DRLSE_2$, respectively.

In our previous work [76], we also proposed an efficient diffusion rate, that achieved the same effect. The function is as follows:

$$D3 = \begin{cases} (|\nabla\phi|^2 - 1)^2 + 2|\nabla\phi|^2(|\nabla\phi|^2 - 1), \\ \qquad 0 < |\nabla\phi| \le 1 \\ 1 - \frac{1}{|\nabla\phi|}, \qquad |\nabla\phi| > 1 \end{cases} \tag{7}$$

In the above diffusion rate, the LSFs can be successfully constrained to a signed distance function. For instance, as shown in Fig. 1, to ensure a flat shape of the LSF, the diffusion rate $D2$ (or $D3$) smoothly decreases $|\nabla \phi|$ to 0 at blue arrow 1 (or black arrow 3), When the value of $|\nabla \phi|$ is larger than 1(as shown by red arrow 2), the diffusion rate is increased to decrease the value of $|\nabla \phi|$, which makes the diffusion rate close to 1.

The variational LSMs without re-initialization have high efficiency in applications [38, 44]. However, some defects exist:

(1) Lower anti-robustness for images with weak boundaries: If an image to be segmented has a weak boundary, the force function will lead to boundary leakage especially near the zero level set. Accordingly, we will obtain an inaccurate segmentation result.
(2) No consideration of the trade-off between the regularization term and segmentation accuracy. In the whole process, the LSFs are always regular and stable; however, the segmentation result will be inaccurate when the energy function converges.
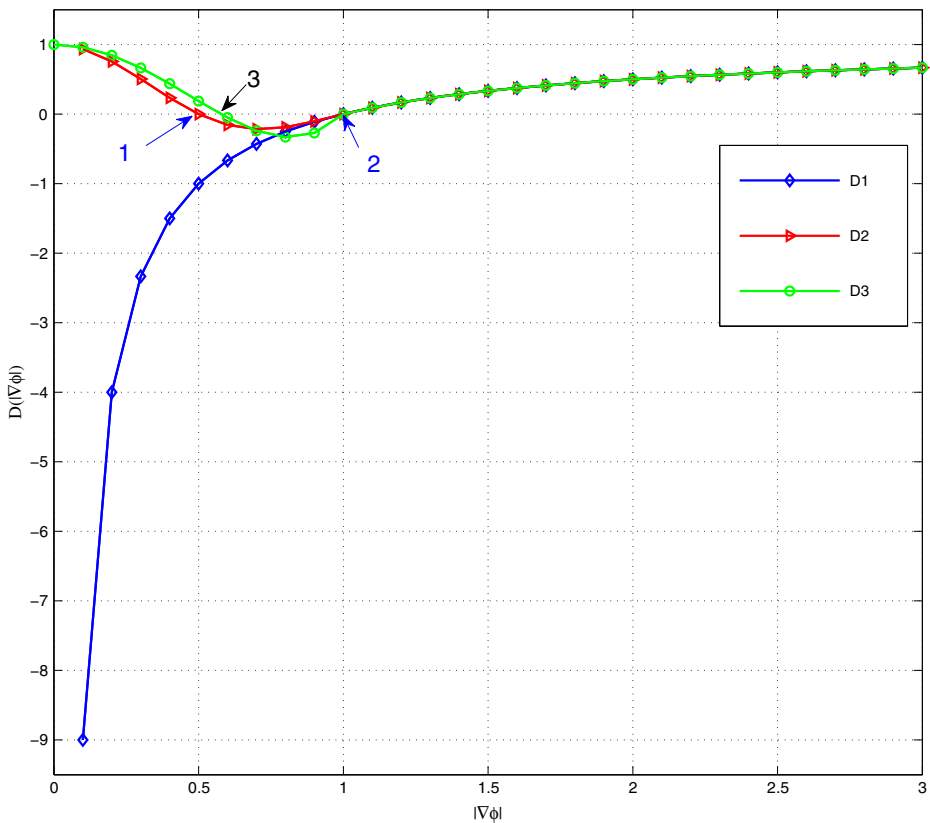
Fig. 1 Comparison of the different diffusion rates

3 Methodology

Despite the drawbacks of the DRLSE method as mentioned above, the model successfully avoids the process of re-initialization and ensures that the level set function has the desired shape in the whole iterative process, as shown in Fig. 2 a. In this paper, we propose an enhanced model to perform accurate segmentation and maintain the LSF as an SDF. Specifically, we first analyse the relationship between the stability of the evolution curve and the accuracy of segmentation. Second, we propose an efficient strategy to achieve a balanced gap. In this strategy. an adaptive perturbation factor is added to the external force to prevent the energy function from falling into a local optimum in the neighbourhood classification process.

3.1 Analysis of curve smoothness and segmentation accuracy

Although LSMs have solved many scientific problems, their applications have always been troubled with the irregularities of the LSF in the curve evolution, which cause numerical errors. Numerical correctness is the guarantee of the stability of the level set [30]. Therefore, to guarantee the stability and numerical computation of the evolution curve, it is critical to

(a) Result of DRLSE

(b)Result of our model
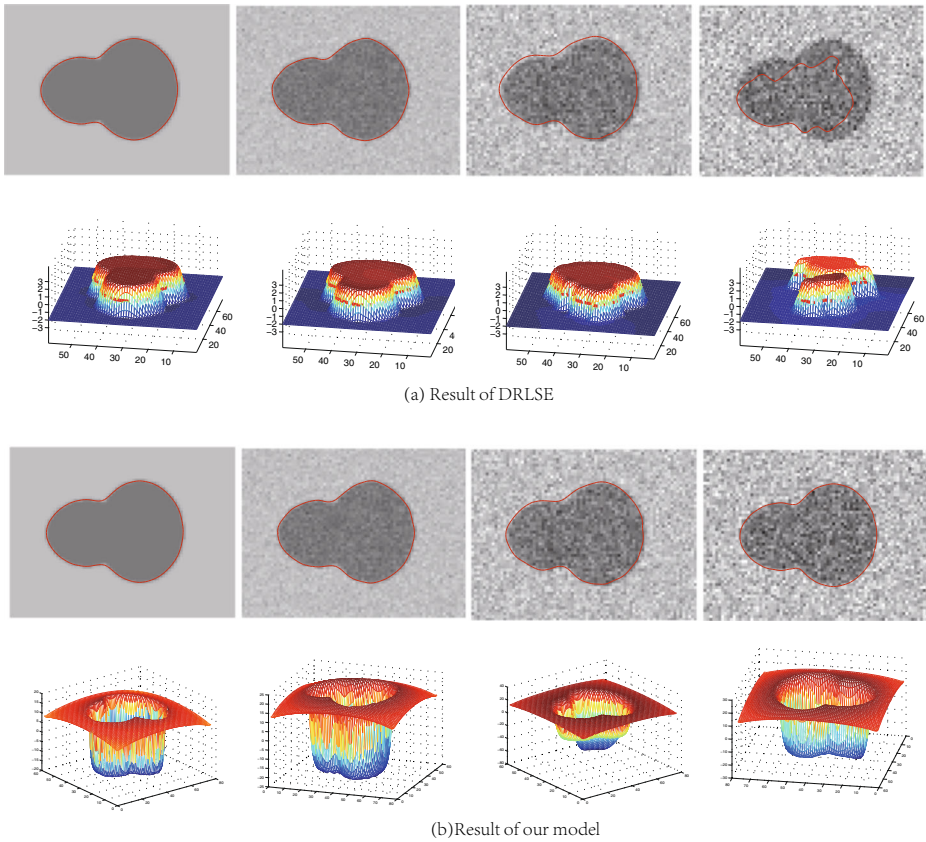
Fig. 2 Comparisons of the influence of regularization term on segmentation accuracy

maintain the property of the signed distance function of the LSF, especially near the zero level set during the evolution process. Accordingly, the LSF should be smooth. However, in the real-world, most images feature intensity inhomogeneity. With the guarantee of the good status of the LSF, accurately segmenting images with intensity inhomogeneity becomes a considerable problem.

As shown in Fig. 2, we perform the segmentation experiments on a synthetic image and its corresponding noisy images. (a) is the segmentation results and their corresponding level sets of the DRLSE model, (b) is the segmentation and their corresponding level sets of the proposed model. In the DRLSE model, the regularization term has a strong smoothing effect and ensures that the LSF has a signed distance property. However, when the intensity value is very similar between the foreground and background, especially near the boundary of the image, the DRLSE model has poor performance. Thus, maintaining the balance between the smoothness of the evolution curve and the accuracy of segmentation is key. Although the LSF of the DRLSE model is more stable, our model performs better than the DRLSE model in segmentation accuracy as shown in Fig. 2b. In our model, we construct an adaptive perturbation strategy to achieve this compromise.

3.2 The proposed model based on the adaptive perturbation factor

As shown in Fig. 2a, When the image noise is severe, the segmentation result is inaccurate, but the regularization function always maintains stability of the level set function under the premise of preserving the image features [35]. With the influence of noise, the LSE force F reaches to a fault balance. In fact, the balance is an illusion. It is vitally important to maintain a balance between the stability of the curve evolution and the accuracy of segmentation. Motivated by perturbation-based methods [9, 16], an adaptive perturbation strategy has the feature of jumping out of the local optimum. In our model, we utilize the perturbation strategy to solve the fault balance. Next, we propose a perturbation factor based level set method to segment images with intensity inhomogeneity. Specifically, an adaptive perturbation factor is added to the external force to disrupt the fake balance in the adaptive iterative process while ensuring the stability of curve evolution. The adaptive perturbation is based on the principle of clustering. In the local neighbourhood regions, the perturbation factor ensures that pixels with similar intensity values belong to the same category. Next, we will elaborate the adaptive model based on the perturbation factor in detail.

In the traditional level set function, the implicit high-dimensional curve evolution function can be expressed as:

$$\begin{cases} \frac{\partial \phi}{\partial t} = F|\nabla \phi| \\ \frac{\partial \phi}{\partial t}|_{t=0} = \phi(x, t = 0) \end{cases} \tag{8}$$

where F is a force function and $\phi(\cdot)$ is a high dimension implicit function, that can handle topological changes in the curve, such as curve merging and splitting. The symbol ∇ is a gradient operator and can be expressed as $\nabla(\cdot) = (\partial(\cdot)/\partial x_1, \partial(\cdot)/\partial x_2, \ldots, \partial(\cdot)/\partial x_n)$, t is a time step.

Motivated by reactive-diffusion methods in chemical mechanisms [12, 22], we propose to add an adaptive perturbation factor to the external force. In the traditional external energy function, noise interference leads to premature convergence of the function during curve evolution. The perturbation strategy can disrupt the fake energy balance. In addition, a regularization term is needed to ensure that the LSF is an SDF. The energy evolution equation is defined as follows:

$$\frac{\partial \phi}{\partial t} = \mu div(D\nabla \phi) + \kappa \alpha^T F|\nabla \phi| + A \cdot \nabla \phi \tag{9}$$

$$\alpha^T = \begin{cases} 1, T \le T_{threshold} \\ exp(-\lambda(I_i - I_j)^2), T > T_{threshold} \end{cases} \tag{10}$$

where μ and κ are two constant parameters, D is a diffusion rate, α^T is a perturbation factor, I_i and I_j are the intensity values at pixels i and j, respectively, F is a scalar function, A represents a vector valued function, T represents the number of iterations, λ is a control parameters, and $T_{threshold}$ is an iteration threshold, in which the curve energy reaches a pseudo-balance due to the effect of factors such as noise. It is difficult to automatically set the threshold for the number of iterations, because the number of iterations is different for different images. The value of t determines the size of the local region. If t is too large , overfitting will occur easily. If t is too small, the result will fall into the local optimum. In the proposed model, after extensive experimental verification, we choose to set t to an empirical value within the narrow band for our experiments. The narrow band will be discussed in Section 3.3.

In details, ideally, if the LSF force F is close to zero, the zero level set will be near the object boundary. However, for an image with intensity inhomogeneity, when the LSF force F is close to zero, the zero level set does not reach the object boundary, because the property of intensity inhomogeneity breaks the balance. The perturbation factor is added to restrict the force function F to act in a small neighbourhood of the zero level set. In fact, the pseudo-balance ensures that the minimization of the energy function falls into the local optimum.

3.3 Implementation

From the analysis in Section 3.2, we realize that the trade-off solution of (10) is a piecewise solving problem, that should be divided into two iterative steps. We call it a two-stage segmentation model based on the perturbation factor. In the first step, a conventional level set with a clipping regularization term is executed; in the second step, an adaptive perturbation factor is added to the external force to prevent the energy function from falling into a local optimum.

In the field of image segmentation, various types of image information can be used to define the energy model. For the level set method, two most important methods are the edge-based method and the region-based method. In our model, we use edge-based information as the external energy. In contrast to the standard edge-base method, we use a perturbation factor to ensure that the misclassification problem falls within the narrow band.

Let I be an image to be segmented on a domain Ω; the conventional edge indicator function g is defined as in (1). Although, the function of $\nabla G_\sigma * I$ in (1) can resist the noise of an image, it also weakens the edge information of the image. Therefore, in our model, we use the next edge indicator function g_i to compensate for the deficiency:

$$g_i = \frac{1}{1 + (g_c/\gamma)^\tau} \tag{11}$$

where g_c is the normalized gradient of I [77], and γ and τ are two constant parameters.

$$g_c = \frac{||\nabla (G_\sigma * I)||}{max||\nabla(G_\sigma * I)||} \tag{12}$$

Let $\phi : \Omega \to \mathcal{R}$, the energy functional $\mathcal{E}_{ext}$ is defined as :

$$\mathcal{E}_{ext} = \lambda \mathcal{L}_g(\phi) + \beta \mathcal{A}_g(\phi) \tag{13}$$

where λ, β are two non-negative parameters. $\mathcal{L}_g$ represents the geometric energy, $\mathcal{A}_g$ is the area weighted function. They are defined as:

$$\mathcal{L}_{g_i}(\phi) = \int_\Omega g_i \delta(\phi)|\nabla \phi| dx \tag{14}$$

and

$$\mathcal{A}_{g_i}(\phi) = \int_\Omega g_i H(-\phi) dx \tag{15}$$

where the Dirac delta function $\delta(\cdot)$ is used to calculate the line integral of g_i, and the Heaviside function $H(\cdot)$ can be used to compute the internal energy of the closed contour. Due to the non-differentiation of the function $H(\cdot)$, we use the approximate function defined as follows:

$$H(x) = \frac{1}{2}\left[1 + \frac{2}{\pi} \arctan\left(\frac{x}{\varepsilon}\right)\right] \tag{16}$$

$$\delta(x) = \frac{\partial H(x)}{\partial x} = \frac{1}{\pi} \cdot \frac{\varepsilon}{\varepsilon^2 + x^2} \tag{17}$$

Combining (9) and (13), we obtain the following energy evolution equation ϕ_t:

$$\phi_t = \mu \, div(D\nabla\phi) + \kappa \alpha^T \lambda \delta(\phi) div\left(g_i \frac{\nabla\phi}{|\nabla\phi|}\right) + \beta g_i \delta(\phi) \tag{18}$$

where μ, κ, β are controlling constant parameters, D and α^T are the diffusion rate and perturbation factor defined in (9) and (10), respectively, and g_i represents the edge detection operator defined in (11). The higher-dimensional implicit function ϕ is a Lipschitz function initialized by the following:

$$\phi_0(x) = \begin{cases} c_0, & x \in \Omega - \Omega_0 \\ 0, & x \in \partial\Omega_0, \\ -c_0, & x \in \Omega_0 - \partial\Omega_0 \end{cases} \tag{19}$$

To reduce the computational cost of the level set method, the proposed model confines the computation within a narrow-band scheme around the closed contour. The red line represents the zero level set, and the narrow-band is between the blue line and the green line. Simply, we define the narrow-band $\mathcal{NB}_\rho$ as follows:

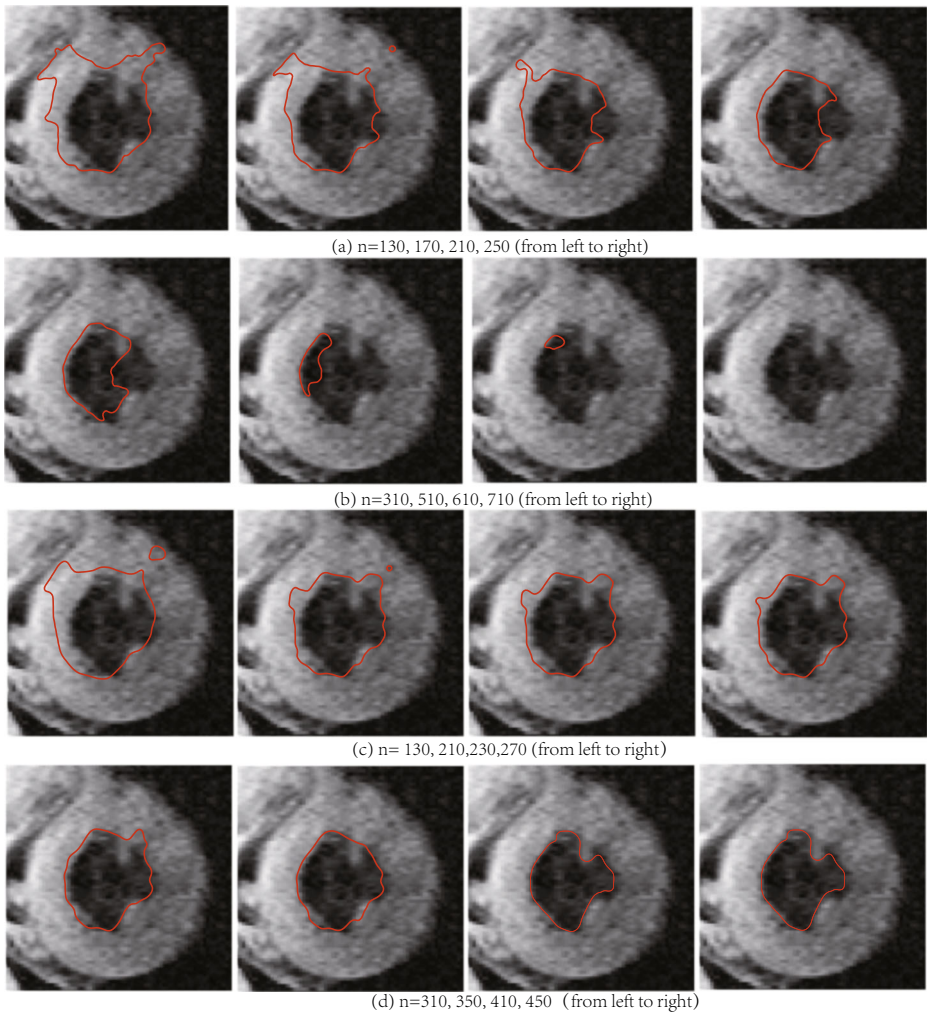$$\mathcal{NB}_\rho = \bigcup_{j \in Z} |i - j|^2 \tag{20}$$

where, Z is the set of points within the narrow-band, j is the neighbourhood centered at pixel i, and ρ is the amplitude of the narrow band. In details, we describe the main steps of our algorithm:

Step 1   Initialization. Initialize the LSF ϕ to be a binary function ϕ_0, and other constant parameters $\mu, \kappa, \lambda, \beta, \varepsilon$ and ρ. Formulate the initial narrow-band according to $\mathcal{NB}_\rho = \bigcup_{j \in Z^0} |i - j|^2$.

Step 2   Compute $\phi^{n+1} = \phi^n + \Delta t L(\phi)$.
         If $t \le T_{threshold}$, update ϕ^{n+1} using (9) ($\alpha^T = 1$); else compute the perturbation factor using (10) within the narrow-band. Then update ϕ^{n+1} using (9).

Step 3   Set the narrow-band using $\mathcal{NB}_\rho^{n+1} = \bigcup_{j \in Z^{n+1}} |i - j|^2$.

Step 4   Convergence judgment. If ϕ^{n+1} satisfies the termination condition, then stop the iteration; otherwise, set $n = n + 1$, go to Step 2.

4 Experimental results

In this section, we will describe experiments to prove the effectiveness of our proposed model for segmenting two-phase medical images. Our experiments are implemented in MATLAB R2013a on a 3.3 GHz Intel. In each experiment, some constant parameters are set as follows: $\Delta t = 1.0, mu = 0.2, k = 1.0, \lambda = 3.0, \beta = 1.0, \rho = 3.0, and \varepsilon = 1.5$. Different values of the time threshold $T_{threshold}$ are used depending on the degree of the intensity inhomogeneity of the image.

In the first experiment, we compare our proposed model with the DRLSE [30] model by applying them to a magnetic resonance(MR) image of the left ventricle of a human heart. The size of the MR image is 136×132 pixels. The image Fig. 3 has severe intensity inhomogeneity, and part of the image boundaries are quite fuzzy. Thus, segmenting this medical image is an arduous task. In Fig. 3a and b show the iterative details of the DRLSE model. In

(a) n=130, 170, 210, 250 (from left to right)

(b) n=310, 510, 610, 710 (from left to right)

(c) n= 130, 210,230,270 (from left to right)

(d) n=310, 350, 410, 450 (from left to right)

Fig. 3 Segmentation Results of DRLSE and Our Model: **a** and **b** are the DRLSE model, **c** and **d** are our model

the first stage, the energy curve evolves along the object(Iteration Times:n=130,170,210), but, due to the severe noise of the MR image and the image smoothing processing, this algorithm causes an error in the segmentation results. In Fig. 4c and d present the segmentation results of the proposed model. The closed contour can converge according to the boundary of the image, eIn particular, for iteration times $n = 310$ as shown in Fig. 4d, the evolution curves converge near the boundary of the image, and finally the energy curves converge at the iteration times $n = 410$ as shown in Fig. 4d. Fig. 4d (n=450) shows that the iteration process has been terminated. From Fig. 6, it can be concluded that the proposed model achieves better segmentation results than the DRLSE model.

To verify the performance of our model in the case of noise, in the second experiment we apply it to a typical ultrasound image with severe noise. For a fair comparison, we use the same initial contour for the ultrasound image. We first use the DRLSE model to
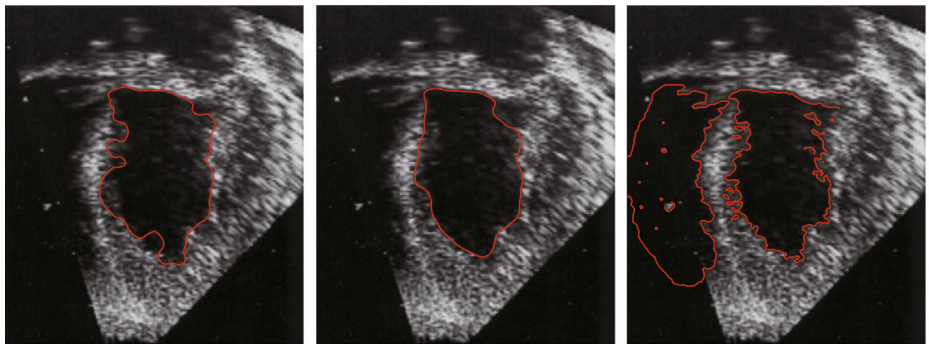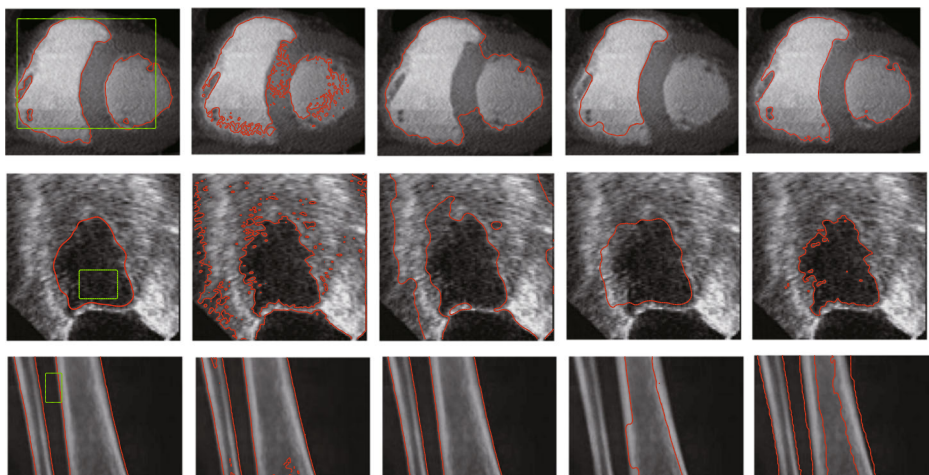
(a) Comparison of DRLSE, our Model and LSACM
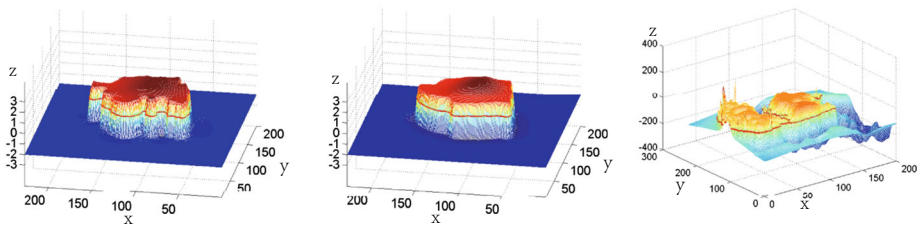
(b) LSF of DRLSE, our Model and LSACM

Fig. 4 Comparisons among Our Model, DRLSE and LSACM

segment the ultrasound image, and the segmentation result is shown in the first part of Fig. 4a. In Fig. 4b, horizontal coordinates (x, y) represent image pixels, and z-axis represents level set function values. The evolution of the LSF is stable as shown in the first part of Fig. 4b, but the segmentation result is less accurate. Due to the influence of severe noise, the energy minimization of the curve falls into the local optimum in the curve evolution process. In addition, the balance between the stability of the LSF and the accuracy of the


Fig. 5 Comparisons among our method, CV, LIF, DRLSE and LSACM(from left to right)

Table 1 CPU time(in s) comparison in Fig. 5

	CPU time				
Figure 5	Our Model	CV	LIF	DRLSE	LSACM
image1(152×128)	28.20	36.18	29.01	42.99	71.40
image2(95×93)	18.63	21.39	22.79	30.46	42.55
image3(87×79)	7.65	15.93	20.32	19.68	39.43

segmentation result is broken in the DRLSE model. Therefore, the DRLSE model has much lower accuracy of segmentation of the ultrasonic image. The second of Fig. 4a shows the segmentation result of our model, which has high accuracy for segmenting the ultrasound image. Compared with the DRLSE model, the advantage of our model is that the adaptive perturbation factor is added to ensure energy minimization into the local optimal solution near the object boundary. In addition, our model guarantee the stability of the LSF as shown in the second of Fig. 4b. As shown in the third part of Fig. 4a the locally statistical active contour model(LSACM) achieves good performance in segmenting images with intensity inhomogeneity, especially magnetic resonance images(see [81] for more details). However, the high noise of the ultrasound image disturbs the distribution of image intensity, and the model is based on the assumption that the noise is a Gaussian distribution with zero mean and variance σ^2. From the third part of Fig. 4b, the model use the standard Von Neumann to assure the stability of the LSF, which is lower than that of DRLSE and our model.

In the third experiment, the segmentation performance of our model is illustrated by comparing it with the Chan-Vese (CV) model [55], local image fitting (LIF) model [78], DRLSE and LSACM(the segmentation results are shown as column 1 to column 5 of Fig. 5,

(a) initial contours   (b) CV model   (c) RSF model   (d)LVC model   (e) Our model
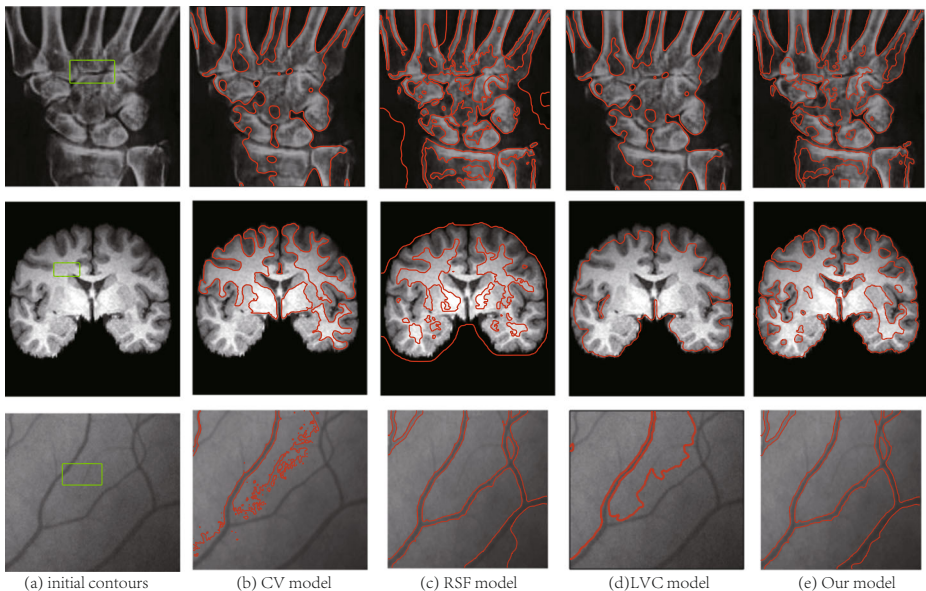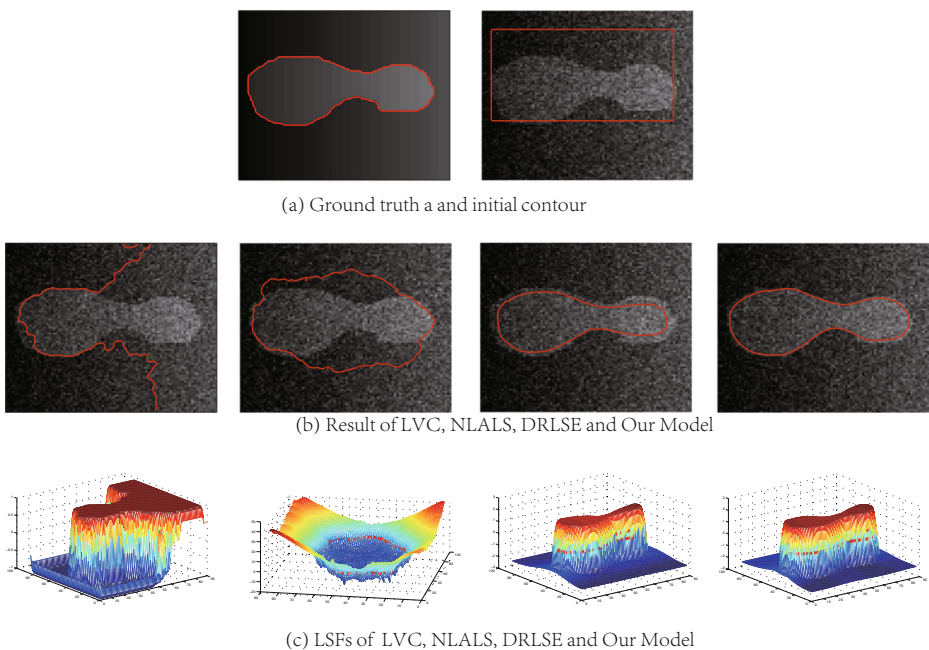
Fig. 6 Comparisons among our method, the CV model, the region-scalable fitting (RSF) [29] model and the local variational contour (LVC) [79] model
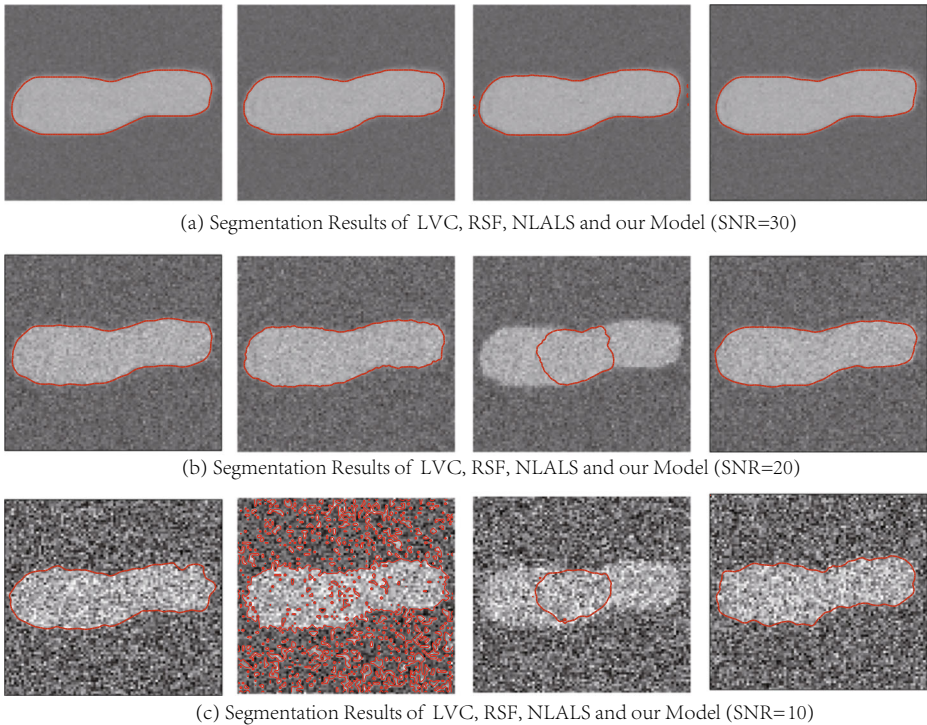
Table 2 CPU time(in s) comparison in Fig. 6

Figure 6	CPU time			
	Our Model	CV	RSF	LVC
image1(160×165)	50.77	185.02	109.07	57.84
image2(141×157)	40.13	91.07	89.55	49.61
image3(181×156)	15.31	175.13	20.02	35.75

respectively). From top to bottom, Fig. 5 shows the segmentation results for a heart CT image, an ultrasound heart image and an X-ray bone image, respectively. In our model, we use a narrow-band as a constraint as shown in (20). The main purpose is to form the local region and clearly state the intensity in each local region. For a fair comparison, for these five models, we use the same initial contour shown in the green window of the first column of Fig. 5. The constant parameters are the optimal scale in all experiments. Table 1 shows the CPU time consumption of the CV, LIF, DRLSE, LSACM and our model. Fig. 5 shows that our model achieves satisfactory results because we attach an adaptive perturbation factor to the external force that can better distinguish each object from the background. The CV model uses global region information and thus misclassifies the medical images with intensity inhomogeneity. The LIF model can adequately segment the bone image because its intensity inhomogeneity is not severe. The DRLSE is stable but does not perform well on these medical images.

To further demonstrate the capability of the proposed model in segmenting images with intensity inhomogeneity in the fourth experiment shown in Fig. 6, we test our model for

(a) Ground truth a and initial contour

(b) Result of LVC, NLALS, DRLSE and Our Model

(c) LSFs of LVC, NLALS, DRLSE and Our Model

Fig. 7 Comparisons among LVC [79], NLALS [58], DRLSE [30] and Our Model

(a) Segmentation Results of LVC, RSF, NLALS and our Model (SNR=30)

(b) Segmentation Results of LVC, RSF, NLALS and our Model (SNR=20)

(c) Segmentation Results of LVC, RSF, NLALS and our Model (SNR=10)

Fig. 8 Comparisons among LVC, RSF, NLALS [58] and Our Model with different signal-noise radio(SNR=30,20,10)

three real medical images. From top to bottom, Fig. 6 shows a bone x-ray image, a brain MRI image and a vessel image, respectively. Table 2 shows the CPU time consumption of the CV, RSF, LVC and our model. Due to the complicated feature of image images, the CV model fails to extract the boundaries of the images and has higher time consumption. The region-scalable fitting (RSF) [29] and the local variational contour (LVC) [79] models can partially segment images. Comparison with the other models, our model is proved to be more efficient.

5 Evaluation

In this section, we first evaluate the stability of curve evolution using a synthetic image in the fourth experiment. In Fig. 7a is the ground truth(left) and the initial contour of the noisy image (right), (b) represents the segmentation results of the LVC [79], the nonlinear adaptive level set (NLALS) [58], the DRLSE [30] and our model, (c) shows the respective level set functions, respectively (from left to right). The results of the comparison show that our model is more stable and accurate.

To evaluation the effectiveness of our model, an effective similarity measurement must be chosen [10, 60]. Among various similarity coefficients, we use the Jaccard similarity coefficient to compare our model with state-of-the-art models, including the LVC [79], RSF [29] and NLALS [58] models. The Jaccard similarity coefficient, also known as the Jaccard

Table 3 Comparisons of Jaccard Index with different signal-noise radio

Models	SNR=10	SNR=20	SNR=30
LVC	0.9808	0.9841	0.9978
RSF	0.5908	0.9821	0.9976
NLALS	0.7198	0.8343	0.9933
Our Model	0.9839	0.9959	0.9981

index(JI), is a statistic used for measuring similarity between finite sample sets. In the field of image segmentation, the JI can be computed by

$$JI(S_1, S_2) = \frac{|S_1 \cap S_2|}{|S_1 \cup S_2|} \tag{21}$$

where S_1 and S_2 are the segmented object region and the ground truth, respectively. Specifically, the larger JI, the more accurate the segmentation rate.

We use a synthetic image with three different signal-to-noise ratio (Fig. 8a SNR=30,(b) SNR=20, and (c) SNR=10) to compare the proposed model with other state-of-the-art models as shown in Table. 3. For a fair comparison, we use the same initial contour in all experiments. When the noise is small, the differences between the models are not obvious, and the JI values are relatively similar, as shown in Fig. 8 (SNR=30). In the three models, the LVC model utilizes Gaussian filter to regularize the LSF and has the capacity of anti-edge leakage, Therefore, the model can well segment noisy image as shown in the first column of Fig. 8; the RSF model constructs a date fitting term by using kernel function, and well segments images with intensity inhomogeneity as shown in the second column of Fig. 8a and b. However, it is hard to control the scale parameter, when the scale parameter is unsuitable, the model has poor performance as shown in the second column of Fig. 8c. And the NLALS construct a clever velocity in the energy functional for objects with weak boundaries, and it performs well in segmenting images with weak boundaries, however, the third column of Fig. 8 shows that this model cannot segment severe noisy images. As the noise increases, the comparison results become more significant. Table 3 shows that LVC has equivalent performance against the proposed, and the proposed model is better than the RSF model and NLALS model. In general, our model is more efficient than other models. The main reason lies in that the adaptive perturbation factor within the narrow-band is constructed during the curve evolution in the proposed model, which prevents the minimization of the energy function from falling into the local optimum. In addition, the regularization term ensures that the LSF retains the signed distance property during the curve evolution.

6 Conclusion and future works

In this paper, we proposed an adaptive perturbation based level set method for medical image segmentation. In the model, an appropriate regularization technique is presented to maintain the level set as a sign distance function, which guarantees the stability of the evolution curve. Then, we built an improved edge-based ACM with local perturbation by using the local intensity information within the narrow-band, resulting in efficient segmentation of medical images with intensity inhomogeneity. Moreover, our model does not re-initialization, which improves the efficiency of our algorithm. Extensive experiments

exploring different aspects using both synthetic images and medical images are provided to evaluate our model, and demonstrated effective improvements of both segmentation and anti-noise ability, compared with other classic models.

In future work, we will explore at least three directions. (1) GPU-based image processing is expected to accelerate the segmentation speed, and thus we will attempt to accelerate our algorithm by using GPU technology [4, 72, 86, 87] or parallel framework [65, 66]. In addition, in the era of cloud computing, we will try to improve the performance of the proposed model using optimization technology [75]. (2) We will attempt to combine our model with other related areas, such as human motion tracking [13, 36, 37], detection technology [68, 69], deep learning methods [40, 41, 70], and PSO-based intelligent algorithms [67, 71] to improve the efficiency of solving the energy minimization problem. (3) We can refer to natural images [14, 42] or video processes [33, 53, 82] and explore the evaluation standard of medical image segmentation.

Publisher's Note   Springer Nature remains neutral with regard to jurisdictional claims in published maps and institutional affiliations.

References

1. Achanta R, Shaji A, Smith K et al (2012) SLIC Superpixels compared to state-of-the-art superpixel methods. IEEE Trans Pattern Anal Mach Intell 34(11):2274–2282
2. Al-Diri B, Hunter A, Steel D (2009) An active contour model for segmenting and measuring retinal vessels. IEEE Trans Med Imaging 28(9):1488–1497
3. Ali H, Badshah N, Chen K et al (2016) A variational model with hybrid images data fitting energies for segmentation of images with intensity inhomogeneity. Pattern Recogn 51:27–42
4. Alsmirat MA, Jararweh Y, Al-Ayyoub M et al (2017) Accelerating compute intensive medical imaging segmentation algorithms using hybrid CPU-GPU implementations. Multimedia Tools and Applications 76(3):3537–3555
5. Becker M, Nijdam N, Magnenat-Thalmann N (2016) Coupling strategies for multi-resolution deformable meshes: expanding the pyramid approach beyond its one-way nature. Int J Comput Assist Radiol Surg 11(5):695–705
6. Boutiche Y, Abdesselam A (2016) Fast algorithm for hybrid region-based active contours optimisation. IET Image Process 11(3):200–209
7. Chae SH, Moon HM, Chung Y et al (2016) Automatic lung segmentation for large-scale medical image management. Multimedia Tools and Applications 75(23):15347–15363
8. Chen X, Udupa JK, Bagci U et al (2012) Medical image segmentation by combining graph cuts and oriented active appearance models. IEEE Trans Image Process 21(4):2035–2046
9. Chen J, Wang Y, Wang DL (2016) Noise perturbation for supervised speech separation. Speech Commun 78:1–10
10. Chen Y, He F, Wu Y et al (2017) A local start search algorithm to compute exact Hausdorff Distance for arbitrary point sets. Pattern Recogn 67:139–148
11. Chitsaz M, Woo CS (2011) Software agent with reinforcement learning approach for medical image segmentation. J Comput Sci Technol 26(2):247–255
12. Cencini M, Lopez C, Vergni D (2003) Reaction-diffusion systems: front propagation and spatial structures. The kolmogorov Legacy in Physics. Springer, Berlin, pp 187–210
13. Cui J, Liu Y, Xu Y et al (2013) Tracking generic human motion via fusion of low-and high-dimensional approaches. IEEE Trans Syst Man Cybern Syst 43(4):996–1002
14. Dai L, Ding J, Yang J (2015) Inhomogeneity-embedded active contour for natural image segmentation. Pattern Recogn 48(8):2513–2529

15. Delingette H, Montagnat J (2001) Shape and topology constraints on parametric active contours. Comput Vis Image Underst 83(2):140–171
16. Du Y, Tsui BMW, Frey EC (2005) Partial volume effect compensation for quantitative brain SPECT imaging. IEEE Trans Medical Imaging 24(8):969–976
17. Feng J, Jiao LC, Zhang X et al (2013) Robust non-local fuzzy c-means algorithm with edge preservation for SAR image segmentation. Signal Process 93(2):487–499
18. Ge Q, Xiao L, Zhang J et al (2012) An improved region-based model with local statistical features for image segmentation. Pattern Recogn 45(4):1578–1590
19. Gong M, Liang Y, Shi J et al (2013) Fuzzy c-means clustering with local information and kernel metric for image segmentation. IEEE Trans Image Process 22(2):573–584
20. Gong M, Tian D, Su L et al (2015) An efficient bi-convex fuzzy variational image segmentation method. Information 293:351–369
21. Grosgeorge D, Petitjean C, Caudron J et al (2011) Automatic cardiac ventricle segmentation in MR images: a validation study. Int J Comput Assist Radiol Surg 6(5):573–581
22. Howard J, Grill SW, Bois JS (2011) Turing's next steps: the mechanochemical basis of morphogenesis. Nat Rev Mol Cell Biol 12(6):392
23. Ivanovska T, Laqua R, Wang L et al (2016) An efficient level set method for simultaneous intensity inhomogeneity correction and segmentation of MR images. Graphics Comput Med Imaging Graph 48:9–20
24. Ji S, Wei B, Yu Z et al (2014) A new multistage medical segmentation method based on superpixel and fuzzy clustering. Comput Math Methods Med 2014:747549
25. Kass M, Witkin A, Terzopoulos D (1988) Snakes: Active contour models. Int J Comput 1(4):321–331
26. Kim JU, Kim HG, Ro YM (2017) Iterative deep convolutional encoder-decoder network for medical image segmentation. In: 2017 39th annual international conference of the IEEE Engineering in Medicine and Biology Society (EMBC). IEEE, pp 685–688
27. Lankton S, Tannenbaum A (2008) Localizing region-based active contours. IEEE Trans Image Process 17(11):2029–2039
28. Li C, Xu C, Gui C et al (2005) Level set evolution without re-initialization: a new variational formulation. In: IEEE computer society conference on Computer Vision and Pattern Recognition, 2005. CVPR 2005. IEEE, vol 1, pp 430–436
29. Li C, Kao CY, Gore JC et al (2008) Minimization of region-scalable fitting energy for image segmentation. IEEE Trans Image Process Publ IEEE Signal Process Soc 17(10):1940
30. Li C, Xu C, Gui C et al (2010) Distance regularized level set evolution and its application to image segmentation. IEEE Trans Image Process 19(12):3243–3254
31. Li C, Huang R, Ding Z et al (2011) A level set method for image segmentation in the presence of intensity inhomogeneities with application to MRI. IEEE Trans Image Process 20(7):2007–2016
32. Li K, He F, Yu HP et al (2017) A correlative classifiers approach based on particle filter and sample set for tracking occluded target. Appl Math-A J Chin Univ 32(3):294–312
33. Li K, He FZ, Yu HP (2017) Robust Visual Tracking based on convolutional features with illumination and occlusion handing. J Comput Sci Technol 33(1):223–236
34. Li K, He F, Yu H, Chen X (2018) A parallel and robust object tracking approach synthesizing adaptive Bayesian learning and improved incremental subspace learning. Frontiers of Computer Science: https://doi.org/10.1007/s11704-018-6442-4
35. Liu YL, Wang J, Chen X et al (2008) A robust and fast non-local means algorithm for image denoising. J Comput Sci Technol 23(2):270–279
36. Liu Y, Cui J, Zhao H et al (2012) Fusion of low-and high-dimensional approaches by trackers sampling for generic human motion tracking. In: 2012 21st International Conference on Pattern Recognition (ICPR). IEEE, pp 898–901
37. Liu Y, Zheng Y, Liang Y et al (2016) Urban water quality prediction based on multi-task multi-view learning. In: Proceedings of the 25th international joint conference on artificial intelligence
38. Liu C, Pan Z, Duan J (2013) New algorithm for level set evolution without re-initialization and its application to variational image segmentation. JSW 8(9):2305–2312
39. Loh PL, Wainwright MJ (2011) High-dimensional regression with noisy and missing data: Provable guarantees with non-convexity. Advances in Neural Information Processing Systems, pp 2726–2734
40. Lu T, Pan L, Jiangs J et al (2017) DLML: Deep Linear mappings learning for face super-resolution with nonlocal-patch. In: Proceedings of the 2017 IEEE International Conference on Multimedia and Expo (ICME). IEEE, pp 1362–1367
41. Luo Y, Zhou L, Wang S et al (2017) Video satellite imagery super resolution via convolutional neural networks. IEEE Geosci Remote Sens Lett 14(12):2398–2402

42. Min H, Jia W, Wang XF et al (2015) An intensity-texture model based level set method for image segmentation. Pattern Recogn 48(4):1547–1562

43. Mumford D, Shah J (1989) Optimal approximations by piecewise smooth functions and associated variational problems. Commun Pur Appl Math 42(5):577–685

44. Ni B, He F, Pan Y et al (2016) Using shapes correlation for active contour segmentation of uterine fibroid ultrasound images in computer-aided therapy. Appl Math A J Chin Univ 31(1):37–52

45. Niu S, Chen Q, de Sisternes L et al (2017) Robust noise region-based active contour model via local similarity factor for image segmentation. Pattern Recogn 61:104–119

46. Oh S, Woo H, Yun S et al (2013) Non-convex hybrid total variation for image denoising. J Vis Commun Image Represent 24(3):332–344

47. Osher S, Sethian JA (1988) Fronts propagating with curvature-dependent speed: algorithms based on Hamilton-Jacobi formulations. J Comput Phys 79(1):12–49

48. Rad AE, Rahim MSM, Kolivand H et al (2017) Morphological region-based initial contour algorithm for level set methods in image segmentation. Multimedia Tools and Applications 76(2):2185–2201

49. Ren Z (2015) Adaptive active contour model driven by fractional order fitting energy. Signal Process 117:138–150

50. Roberts JD (1980) Linear model reduction and solution of the algebraic Riccati equation by use of the sign function. Int J Control 32(4):677–687

51. Ros G, Sellart L, Materzynska J et al (2016) The synthia dataset: a large collection of synthetic images for semantic segmentation of urban scenes. Proc IEEE Conf Comput Vis Pattern Recognit, pp 3234–3243

52. Shang Y, Deklerck R, Nyssen E et al (2011) Vascular active contour for vessel tree segmentation. IEEE Trans Biomed Eng 58(4):1023–1032

53. Shao L, Cai Z, Liu L et al (2017) Performance evaluation of deep feature learning for RGB-d image/video classification. Inf Sci 385:266–283

54. Tian Y, Duan F, Zhou M et al (2013) Active contour model combining region and edge information. Mach Vision Appl 24(1):47–61

55. Vese LA, Chan TF (2002) A multiphase level set framework for image segmentation using the Mumford and Shah model. Int Journal Comput Vision 50(3):271–293

56. Wang B, Gao X, Tao D et al (2010) A unified tensor level set for image segmentation[J]. IEEE Trans Syst Man Cybern B Cybern 40(3):857–867

57. Wang XF, Huang DS, Xu H (2010) An efficient local Chan Vese model for image segmentation. Pattern Recogn 43(3):603–618

58. Wang B, Gao X, Tao D et al (2014) A nonlinear adaptive level set for image segmentation. IEEE Trans Cybern 44(3):418–428

59. Wang H, Huang TZ, Xu Z et al (2014) An active contour model and its algorithms with local and global Gaussian distribution fitting energies. Inf Sci 263:43–59

60. Wang XF, Min H, Zou L et al (2015) A novel level set method for image segmentation by incorporating local statistical analysis and global similarity measurement. Pattern Recogn 48(1):189–204

61. Weickert J, Kühne G (2003) Fast methods for implicit active contour models. Geometric level set methods in imaging, vision, and graphics. Springer, New York, pp 43–57

62. Xu C, Prince JL (1998) Snakes, shapes, and gradient vector flow[J]. IEEE Trans Image Process 7(3):359–369

63. Xue DX, Zhang R, Zhao YY et al (2017) Fully convolutional networks with double-label for esophageal cancer image segmentation by self-transfer learning. In: Ninth International Conference on Digital Image Processing (ICDIP 2017). International Society for Optics and Photonics 10420, p 104202D

64. Yan P, Zhang W, Turkbey B et al (2013) Global structure constrained local shape prior estimation for medical image segmentation. Comput Vis Image Underst 117(9):1017–1026

65. Yan C, Zhang Y, Xu J et al (2014) Efficient parallel framework for HEVC motion estimation on many-core processors. IEEE Trans Circ Syst Video Technol 24(12):2077–2089

66. Yan C, Zhang Y, Xu J et al (2017) A highly parallel framework for HEVC coding unit partitioning tree decision on many-core processors. IEEE Signal Process Lett 21(5):573–576

67. Yan XH, He FZ, Chen YL (2017) A novel hardware/software partitioning method based on position disturbed particle swarm optimization with invasive weed optimization. J Comput Sci Technol 32(2):340–355

68. Yan C, Xie H, Liu S et al (2018) Effective Uyghur language text detection in complex background images for traffic prompt identification. IEEE Trans Intelli Transp Syst 19(1):220–229

69. Yan C, Xie H, Chen J et al (2018) An effective Uyghur text detector for complex background images. IEEE Transactions on Multimedia. https://doi.org/10.1109/TMM.2018.2838320

70. Yan C, Xie H, Yang D et al (2018) Supervised hash coding with deep neural network for environment perception of intelligent vehicles. IEEE Trans Intell Transp Syst 19(1):284–295

71. Yan X, He F, Hou N et al (2018) An efficient particle swarm optimization for large-scale hardware/software co-design system. Int J Coop Inf Syst 27(01):741001
72. Yang XJ, Liao XK, Lu K et al (2011) The TianHe-1A supercomputer: its hardware and software. J Comput Sci Technol 26(3):344–351
73. Yang L, Meer P, Foran DJ (2005) Unsupervised segmentation based on robust estimation and color active contour models. IEEE Trans Inf Technol Biomed 9(3):475–486
74. Yang X, Gao X, Tao D et al (2014) Improving level set method for fast auroral oval segmentation. IEEE Trans on Image Process 23(7):2854–2865
75. Yang Z, Jia D, Ioannidis S et al (2018) Intermediate Data Caching Optimization for Multi-Stage and Parallel Big Data Frameworks. arXiv:1804.10563
76. Yu H, He F, Pan Y et al (2016) An efficient similarity-based level set model for medical image segmentation. J Adv Mech Des Syst Manuf 10(8):JAMDSM0100–JAMDSM0100
77. Yushkevich PA, Piven J, Hazlett HC et al (2006) User-guided 3D active contour segmentation of anatomical structures: significantly improved efficiency and reliability. Neuroimage 31(3):1116–1128
78. Zhang K, Song H, Zhang L (2010) Active contours driven by local image fitting energy. Pattern Recog 43(4):1199–1206
79. Zhang K, Zhang L, Song H et al (2010) Active contours with selective local or global segmentation: a new formulation and level set method. Image Vision Comput 28(4):668–676
80. Zhang N, Ruan S, Lebonvallet S et al (2011) Kernel feature selection to fuse multi-spectral MRI images for brain tumor segmentation. Comput Vis Image Underst 115(2):256–269
81. Zhang K, Zhang L, Lam KM et al (2016) A level set approach to image segmentation with intensity inhomogeneity. IEEE Trans Cybern 46(2):546–557
82. Zhang T, Ghanem B, Liu S et al (2016) Robust visual tracking via exclusive context modeling. IEEE Trans Cybern 46(1):51–63
83. Zhang D, He F, Han S et al (2017) An efficient approach to directly compute the exact Hausdorff distance for 3D point sets. Integr Comput Aided Eng 24(3):261–277
84. Zhao Y, Rada L, Chen K et al (2015) Automated vessel segmentation using infinite perimeter active contour model with hybrid region information with application to retinal images. IEEE Trans Med Imaging 34(9):1797–1807
85. Zhou Y, Xu H, Pan X et al (2016) Parsing main structures of indoor scenes from single RGB-D image. J Adv Mech Des Syst Manuf 10(8):JAMDSM0102-JAMDSM0102
86. Zhou Y, He F, Qiu Y (2017) Dynamic strategy based parallel ant colony optimization on GPUs for TSPs. Sci China Inf Sci 60(6):068102
87. Zhou Y, He F, Hou N et al (2018) Parallel ant colony optimization on multi-core SIMD CPUs. Futur Gener Comput Syst 79:473–487
88. Zhou S, Wang J, Zhang M et al (2017) Correntropy-based level set method for medical image segmentation and bias correction. Neurocomputing 234:216–229

Haiping Yu is currently a Ph.D. Candidate at the school of computer science in Wuhan University. Her research interests are pattern recognition, image processing and computer graphics.

Fazhi He received Ph.D. Degree from Wuhan University of Technology. He was post-doctor researcher in The State Key Laboratory of CAD & CG at Zhejiang University, a visiting researcher in Korea Advanced Institute of Science & Technology and a visiting faculty member in the University of North Carolina at Chapel Hill. Now he is a professor in School of Computer, Wuhan University. His research interests are Computer Graphics, Computer-Aided Design, Image Processing and Computer Supported Cooperative Work.

Yiteng Pan is currently a Ph.D Candidate at the School of Computer Science in Wuhan University. His research interests include data mining, image processing and deep learning.